Title

Impact of Surface Adsorption on DNA Structure and Stability: Implications for Environmental DNA Interactions with Iron Oxide Surfaces.

Journal

Langmuir, 40(52)

Authors

Hettiarachchi, Eshani

Grassian, Vicki

Publication Date

2024-12-31

DOI

10.1021/acs.langmuir.4c02501

Peer reviewed

LANGMUIR

pubs.acs.org/Langmuir
Article

Impact of Surface Adsorption on DNA Structure and Stability: Implications for Environmental DNA Interactions with Iron Oxide Surfaces

Published as part of Langmuir special issue "Highlighting Contributions from our Editorial Board Members in 2024".

Eshani Hettiarachchi and Vicki H. Grassian*

Cite This: *Langmuir* 2024, 40, 27194−27205

Read Online

ACCESS | Metrics & More | Article Recommendations | Supporting Information

ABSTRACT: Environmental DNA (eDNA), i.e., DNA found in the environment, can interact with various geochemical surfaces, yet little is known about these interactions. Mineral surfaces may alter the structure, stability, and reactivity of eDNA, impacting the cycling of genetic information and the reliability of eDNA-based detection tools. Understanding how eDNA interacts with surfaces is crucial for predicting its fate in the environment. In this study, we examined the surface interaction and stability of herring testes DNA, a model system for eDNA, on two common iron oxide phases present in the environment: α-FeOOH (goethite) and α-Fe_2O_3 (hematite). Utilizing spectroscopic probes, including attenuated total reflection Fourier-transform infrared (ATR-FTIR) and UV−vis spectroscopy, we quantified the DNA adsorption capacity at pH 5 and determined its secondary structure. DNA adsorbed irreversibly at pH 5 and 25 °C, primarily through its phosphate groups, and retained the solution-phase B-form structure. However, the infrared data also indicated some distortion of the B-form likely due to additional interactions between nitrogenous bases when adsorbed on the α-Fe_2O_3 particle surfaces. The distortion in the double helical structure of adsorbed DNA on α-Fe_2O_3 led to a lower melting temperature (T_m) of 60 °C compared to 70 °C for DNA in solution. In contrast, DNA adsorbed on α-FeOOH melted at higher temperatures relative to solution-phase DNA and in two distinct phases. Upon testing adsorbed DNA stability at higher pH values, there were distinct differences between the two iron oxide phases. For α-FeOOH, nearly 50% of the DNA desorbed from the surface when the solution pH changed from 5 to 8, while less than 5% desorbed from α-Fe_2O_3 under the same conditions. Overall, these findings underscore the importance of mineral-specific eDNA−surface interactions and their role in adsorbed eDNA stability, in terms of DNA melting and the impact of solution-phase pH changes.

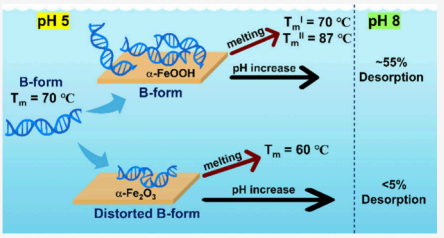

INTRODUCTION

Environmental DNA (eDNA) refers to the total DNA pool found in the environment.[1−4] This includes DNA found in waterbodies, sediments, soil, rocks and minerals, air, and organismal DNA present at the collection of the environmental samples.[2,4,5] In recent years, eDNA-based species detection and monitoring techniques have become appealing due to being noninvasive, rapid, and cost-effective and requiring no physical observation to extract biodiversity information.[1−3,6−10] For example, eDNA-based detection methods are used to identify the species profile of the locale, presence of invasive and pathogenic species, and species migration through environments.[2,3,10,11] Additionally, eDNA-based research is conducted in paleobiology and paleontology in order to understand paleospecies profiles and past biodiversity.[12] However, these eDNA-based detection and monitoring tools rely on our understanding of DNA chemistry and retention time in various environmental conditions and on our ability to design more method-diverse monitoring tools.[6,8]

Once a species sheds DNA into a water system, it is known as extraorganismal eDNA.[1,13] Extraorganismal eDNA can stay in the environment as dissolved eDNA, eDNA bound to the surfaces of suspended and sedimented particles, and eDNA still encapsulated in cells or organelles.[1,10,13] In many environmental samples, eDNA is separated out as particles. Several studies show the size range of eDNA particles can vary across a wide range of sizes from 0.2 to 180 μm indicating a large range of eDNA fragment sizes.[14−18]

When eDNA is adsorbed on mineral surfaces, it has been suggested that it may be stabilized on the surface by lowering kinetic decay rates and that surfaces may protect adsorbed

Received: July 1, 2024
Revised: October 11, 2024
Accepted: November 26, 2024
Published: December 19, 2024

https://doi.org/10.1021/acs.langmuir.4c02501
Langmuir 2024, 40, 27194−27205

eDNA molecules by rendering specific moieties unavailable for reactivity within DNA, including from hydrolysis, photochemistry, and oxidation.[10,19−21] However, it is also possible that some mineral surfaces can act as catalysts and promote degradation of adsorbed eDNA.[10,20,22−25] Thus, the effects associated with DNA−mineral surface interactions may vary widely and depend on specific mineral surface properties as well as the nature of the aquatic environment, such as the pH, temperature, other chemical and biological species present, and the availability of solar radition.[1,2,10,26]

The adsorption/desorption, reactivity, and retention of eDNA on different mineral surfaces are therefore of great interest because of the persistence of possibly mutated/degraded DNA in the environment and cycling of genetic information.[27,28] Moreover, migration of eDNA from one locale to another in bound forms can affect the accuracy of eDNA monitoring techniques.[27] The latter is more concerning in marine and brine environments, where the elevated pH (∼8) may cause desorption of eDNA adsorbed on suspended particles in freshwater systems at lower pH (∼5−6). Additionally, nucleic acid interactions on mineral surfaces are an important aspect of the prebiotic origin of an RNA world, as well as in the search of extraterrestrial life.[21,24,25,27] Thus, understanding specific details of eDNA−mineral interactions in various natural environments is paramount to broaden our knowledge and to strengthen our capacity of eDNA-based environmental detection and monitoring tools for both present and past particle-bound eDNA systems. For example, understanding these mineral-specific differences and similarities in various environments may provide insights into designing improved eDNA recovery and extraction protocols to be used in species profiling.

There have been several studies conducted on the adsorption of nucleic acid components, such as nucleotides. These include guanine (G), adenine (A), cytosine (C), and thymine (T) on minerals such as goethite (α-FeOOH), hematite (α-Fe_2O_3), rutile (TiO_2), and ceria (CeO_2).[29−33] These studies show that the primary interaction site of these molecules is the negatively charged phosphate groups, via both inner and outer sphere complexation.[29−33] In an earlier study, we reported that nucleotides with purine bases (G and A) preferentially adsorbed on TiO_2 over their pyrimidine counterparts (C and T), indicating a higher affinity of G and A bases toward the surface.[30] In another study following the adsorption of DNA on α-FeOOH particle surfaces, it was determined that adsorption through phosphate groups occurred with no degradation or disruption to the helical structure.[28] Additionally, DNA adsorption on clay minerals suggests the involvement of electrostatic forces, cation bridging, and ligand exchange.[20,23] One simulated study on DNA taphonomy, however, shows the possibility of nitrogenous bases interacting with these surfaces upon adsorption, particularly G residues.[34] Despite their importance, our understanding of eDNA adsorption pathways on these environmentally relevant interfaces and their impact on reactivity and retention of adsorbed eDNA in the environment remain largely unexplored.

In the current study, we employed herring testes DNA, a well understood fish DNA, as a model system to investigate eDNA interactions and adsorption pathways with two common iron oxide mineral phases, α-FeOOH and α-Fe_2O_3, under environmentally relevant conditions, using ATR-FTIR and UV−vis spectroscopy. Herring fish is a type of fish that lives in both freshwater and saltwater systems and is abundant in natural environment.[35,36] Fresh water systems are within the pH range of 5−6, so in this study we kept the solutions at pH 5 so as to be within the appropriate pH range. Our study aims to address several questions. First, does the DNA structure change upon adsorption? Second, once adsorbed, how do changes in pH affect DNA adsorption and stability? Third, how does surface adsorption impact DNA thermal stability? Fourth, do different minerals impact surface DNA adsorption and DNA stability with respect to the pH and temperature differently? Overall, this study seeks to further our understanding of eDNA interactions with environmentally relevant geochemical interfaces and mineral specific eDNA surface interactions.

MATERIALS AND METHODS

Materials. Double-stranded herring testes DNA (B-form, type XIV, Sigma-Aldrich, product no. D6898, maximum length ∼1000 base pairs) was used as received in all experiments. Sodium chloride (NaCl, Fisher Scientific) was used for ionic strength adjustments. Hydrochloric acid (HCl, 1 N, Fisher Scientific) and sodium hydroxide (NaOH, 1 N, Fisher Scientific) were used as received for pH adjustments. Deionized water (Milli-Q, 18.2 MΩ) was used in all solution preparations. Iron(III) oxide (hematite, α-Fe_2O_3, nano powder, Thermo Scientific, 30−50 nm, APS, BET surface area 123 ± 5 m^2 g^{-1}) and iron(III) hydroxide (goethite, α-FeOOH, nanopowder, Alfa Aesar, 320 ± 140 and 21 ± 9 nm,[37] BET surface area 17 ± 1 m^2 g^{-1}) were used in thin film preparation.

Point of Zero Charge (pzc) Determination via pH Drift Method. The pzc of the different iron oxide particles in 30 mM NaCl solutions was estimated via pH drift method.[38] Briefly, a pH series of 30 mM NaCl solutions (10 mL) were prepared between pH 3 and pH 12. Then 50 mg of either α-FeOOH or α-Fe_2O_3 was added to these solutions and slowly mixed for 2 h and the final pH was recorded. The pzc is where $pH_{initial} - pH_{final} = 0$. For these samples, the pzc was determined to be 8.4 and 7.0 for α-FeOOH or α-Fe_2O_3, respectively, which agrees with previously published studies.[39]

Preparation of DNA Solutions in B-Form Double Stranded DNA (dsDNA) and Single Stranded DNA (ssDNA). For solution phase and adsorption infrared measurements, 5 mg mL^{-1} and 0.5 mg mL^{-1}, respectively, of DNA solutions in 30 mM NaCl were prepared via vortex mixing. Previous research has shown the effect of ionic strength on the kinetics of DNA adsorption.[40] Here 30 mM NaCl was chosen to maintain a constant ionic strength and to mimic the low salt concentrations in freshwater systems. For the B-form double stranded DNA (dsDNA), the desired mass of DNA threads was dissolved in 30 mM NaCl solutions and then the pH was adjusted to 5. For the single stranded DNA (ssDNA) a 10 mL of B-form DNA solution in 30 mM NaCl at pH 5 from above was heated at 95 °C for 3 min in an Erlenmeyer flask to induce the formation of ssDNA through thermal denaturation of dsDNA. This is enough thermal energy to break the H-bonds holding the two DNA strands together, a process known as DNA melting.[41]

Surface Coverage Measurements Using UV−visible Spectroscopy. DNA surface coverages at pH 5 on the two iron oxide phases were determined by using UV−vis absorption spectroscopy. 10 mg of α-FeOOH or α-Fe_2O_3 was added to a 2 mL of 0.5 mg mL^{-1} DNA solution at pH 5 and slowly mixed in a rotor for 2 h at 3.4 rpm. Then, the mixture was centrifuged to separate the supernatant from the solid residue which contains the oxide particles and adsorbed DNA, using a Thermo Fisher Scientific Sorvall biofuge stratos centrifuge at 10k revolutions per minute (RPM) for 2 min and with a relative centrifugal force (RCF) of 1.118×10^4. The solid residue was mixed with another fresh 2 mL of 0.5 mg mL^{-1} DNA solution sample, and the process was repeated until the DNA concentrations in the final supernatants were constant, indicating the surface concentration was in equilibrium with the solution. The UV absorbance at 260 nm of supernatants was measured, and the DNA concentrations were

https://doi.org/10.1021/acs.langmuir.4c02501
Langmuir 2024, 40, 27194−27205

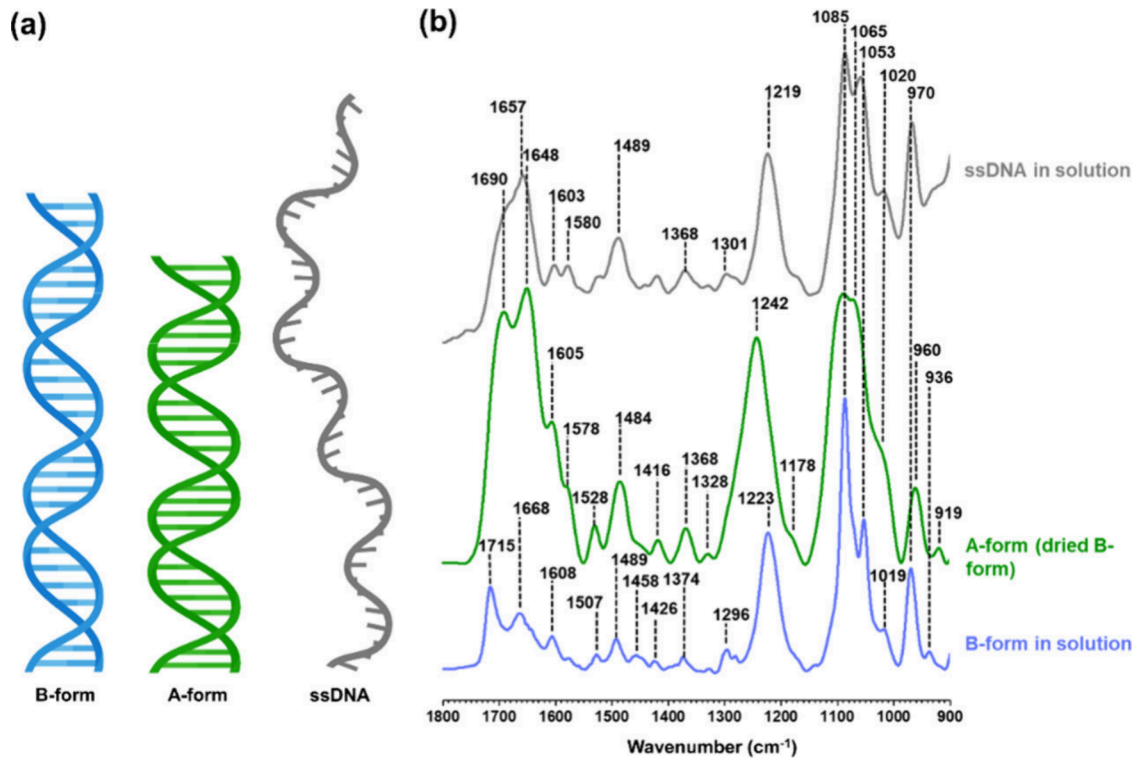

Figure 1. (a) Pictorial representation of different DNA forms including double stranded B- and A-forms and ssDNA; (b) ATR-FTIR spectra in the spectral region extending from 900 to 1800 cm^{-1} of solution phase B-form, A-form (dried B-form), and solution phase ssDNA form.

determined using a calibration curve. The initial DNA concentration was also determined through the same process. The amount of adsorbed DNA was calculated by taking the difference of initial DNA concentration and supernatant DNA concentration. The experiments were done in triplicate.

Attenuated Total Reflection Fourier Transform Infrared Spectroscopy (ATR-FTIR) for DNA Interactions on Iron Oxide Particle Surfaces. A detailed description of the setup and fundamentals of ATR-FTIR measurements have been described previously.[42] A horizontal flow cell ATR accessory from PIKE Tech with either zinc selenide (ZnSe) or an amorphous material transmitting IR radiation (AMTIR) crystal was placed inside the internal compartment of the FTIR spectrometer (Nicolet iS10). Infrared spectra were collected with a mercury cadmium telluride detector (MCT/A), at a resolution of 4 cm^{-1} and averaged over 100 scans.

Solution-phase spectra of DNA solutions on the ZnSe crystal were taken to observe any spectral changes compared to adsorbed DNA onto α-FeOOH and α-Fe_2O_3. ZnSe crystal gave better solution phase spectra in terms of signal-to-noise in the spectral region analyzed, whereas AMTIR crystal showed higher quality spectra for adsorbed DNA. For these experiments, a background spectrum of bare ZnSe crystal was collected. Second, a background spectrum of 30 mM NaCl (800 μL) at pH 5 was taken after purging atmospheric gases out of the sample chamber for approximately 30 min. Then, 800 μL of the 5 mg mL^{-1} DNA solution was pipetted onto the crystal, and a spectrum was collected after purging for an additional 10 min. Additionally, DNA was allowed to dry onto the ZnSe crystal by purging the chamber with dry air (free of CO_2 and H_2O) and another spectrum was collected to get the dried A-form spectrum of the DNA (*vide infra*).

For infrared measurements of adsorbed DNA, α-FeOOH or α-Fe_2O_3 thin films were prepared by sonicating 2 mg of either α-FeOOH or α-Fe_2O_3 in 1 mL of Milli-Q water and then drop-casted these hydrosols containing the particles onto an AMTIR crystal. For α-FeOOH, 200 μL of the hydrosol was determined to be the optimal amount of particles needed without saturation of the infrared signal. For both samples, the hydrosol was left to dry overnight, leaving a thin film. To remove any loosely bound α-FeOOH or α-Fe_2O_3 particles, a flow of the 30 mM NaCl solution at pH 5 with a peristaltic pump at 0.8 mL min^{-1} for 20 min over the thin film of particles was initiated before a background scan was recorded. Following background collection, a flow of 0.5 mg mL^{-1} DNA solution (B-form) at pH 5 over the thin film at a rate of 0.8 mL min^{-1} was started. Infrared spectra were collected every 70 s for 1 h. Following this, infrared spectra were then collected for a flow of a solution of 30 mM NaCl solution at pH 5 without DNA for an additional hour. These data were used to monitor both the adsorption and desorption processes to determine if DNA stayed adsorbed onto the particle surface. The thin film containing the particles with adsorbed DNA was then exposed to 30 mM NaCl at pH 8 and 10 for 60 min each by flowing each solution at 0.8 mL min^{-1} over the film while collecting spectra every 70 s. The particle thin film was then allowed to dry by purging the chamber with dry air, and a spectrum was collected. Additionally, in a different set of experiments, after flowing 30 mM NaCl at pH 5 to remove loosely adsorbed DNA onto the surface, the thin film was allowed to dry by purging the chamber with dry air, and a spectrum of dried thin film with adsorbed DNA was collected. Then, another cycle of 30 mM NaCl at pH 5 was flowed over the dried thin film for 60 min while the spectra were collected every 70 s to understand the regeneration capability of dried adsorbed DNA to hydrated DNA at pH 5. It should be noted that these thin films naturally contain particle aggregates, and there is no obvious additional aggregation upon flowing solutions containing DNA or NaCl.

DNA melting curves for both solution-phase and adsorbed-phase DNA were determined using temperature-controlled ATR-FTIR spectroscopy. In these experiments, a heated ATR flow-through cell (HATR) with either ZnSe or AMTIR crystals coupled to PIKE Tech TempPRO 7 software was used. For solution-phase experiments, 30 mM NaCl background and DNA (B-form) solution-phase spectra were collected at temperatures between 25 and 100 °C. These spectra were used to determine the melting temperature (T_m) of DNA (B-form) in solution. On α-FeOOH and α-Fe_2O_3 surfaces, first, 30 mM

https://doi.org/10.1021/acs.langmuir.4c02501
Langmuir 2024, 40, 27194−27205

Table 1. Vibrational Frequencies in cm^{-1} and Peak Assignments for Herring Testes DNA in Solution, Dried, and Adsorbed on Two Iron Oxide Phases

solution phase B-form	dehydrated A-form (dried solution)	solution phase ssDNA	B-form adsorbed on α-FeOOH	B-form adsorbed on α-Fe_2O_3	peak assignments (see refs 28, 49−51, 53, 54)
936	919		936[a]	936	AT base pairs in B-form
970	960	970	970	970	DNA backbone, main chain vibrations
1019	1020	1020	1023	1019	Furanose vibrations
1053	1070	1065	1054	1055	
1085	1085	1085	1088	1090	Symmetric stretching of PO_2^- marker
1223	1242	1219	1217	1222	Asymmetric stretching of PO_2^- marker
1280			1280	1280[a]	Thymidine (dT) in C2′-endo/anti conformation
1296		1301	1296		C_4NH_2 of C
1374	1368	1368	1374	1374	CH_3 symmetric deformation of dT and purine in anti-conformation (C2′/C3′ endo)
1426	1416		1426	1421	C2′ endo deoxyribose puckering in B-form
1458					A bases in B-form
1489	1484	1489	1490	1492	Ring vibrations of A and G bases
1507			1507		In-plane vibrations of C in the rings
1578	1578	1580	1578		Ring C═N vibrations of G, enhanced in ssDNA
1608	1605	1603	1606	1609	C═O bond vibrations of different base pairs. For ssDNA, loss of 1715 (G*G-C/ts), increase of 1690 C2═O2, T, 1659 C2═O2, C), 1580 (C═N ring vibration of G), 1603 (ring vib of purines)
1668	1648	1657	1653	1640	
1715			1711	1715	

[a]Observed as a shoulder.

NaCl backgrounds at pH 5 were collected at different temperatures between 25 and 100 °C. Once the HATR accessory is cooled to room temperature, 0.8 mL min^{-1} flow rate of 0.5 mg mL^{-1} DNA (B-form) solution began to flow and continued for 60 min. This was followed by 30 mM NaCl at pH 5 so that only adsorbed DNA was on the surface. Spectra were then collected as the temperature of the cell was increased with a temperature ramp set to 5 °C increments (except for including 87 °C) utilizing a heating rate of 1 °C/min and with an equilibration time of 600 s. The ATR-FTIR spectra collected at different temperatures were used to determine the T_m. Spectra were analyzed utilizing single value decomposition (SVD) and principle component analysis (PCA).[43−46] Detailed information on this matrix decomposition from SVD/PCA is provided elsewhere.[43−46] SVD was performed with Python programming, for a matrix $n \times m$, where n/ rows represent the spectral region of interest, 900−1800 cm^{-1}, and m/columns represent the absorbance for each wavenumber at different temperatures. The Python program was written and run on Jupyter Notebooks[47] and provided in the Supporting Information (SI). The raw data were fit to a two-state Boltzmann formula to generate the respective melting curve, as discussed in more detail below and in the SI.

RESULTS AND DISCUSSION

Surface Coverages of DNA at pH 5 on α-FeOOH and α-Fe_2O_3. Surface coverages of DNA adsorbed onto two different mineral surfaces, α-FeOOH and α-Fe_2O_3, at pH 5 were determined. The maximum surface coverage of DNA on α-FeOOH surfaces at pH 5 was 46 ± 2 mg of DNA per 1 g of α-FeOOH (SI−Figure S1). Similarly, maximum surface coverages were determined for α-Fe_2O_3 surfaces at pH 5 and were 39 ± 1 mg of DNA per 1 g of α-Fe_2O_3, respectively. Although these values are somewhat similar on a per mass basis, the surface area normalized maximum surface coverage for α-FeOOH and α-Fe_2O_3 is 2.7 ± 0.10 and 0.32 ± 0.04 mg m^{-2}, respectively, differing by nearly 1 order of magnitude, suggesting differences in DNA interactions. For these surface coverage measurements, the masses used in thin film preparation for ATR-FTIR experiments are different (2 mg for α-Fe_2O_3 and 0.4 mg for α-FeOOH). The amount of DNA adsorbed on each surface under these mass conditions at the end of 1 h exposure is 0.11 ± 0.01 mg and 0.13 ± 0.01 mg for α-Fe_2O_3 and α-FeOOH, respectively. Since the pzc is above pH 5, α-FeOOH (~8.4) and α-Fe_2O_3 (~7.0), both surfaces are positively charged, which facilitates electrostatic interactions with negatively charged DNA. In addition, both surfaces are fully protonated. At higher pH above the pzc, these surfaces will become negatively charged and contain both protonated and deprotonated surface sites.

Solution Phase ATR-FTIR Spectroscopy of Different Forms of DNA. ATR-FTIR spectroscopy of different structural forms of DNA double stranded (ds) and single stranded (ss) DNA was first measured. In particular, the infrared spectra of the B- and A-forms of dsDNA and ssDNA were collected. Figure 1a shows a pictorial representation of the structures of these forms and the corresponding ATR-FTIR spectra (Figure 1b). The B-form is stable in most natural environments under circumneutral pH. Upon dehydration, the B-form converts to the A-form.[48−51] These infrared spectra provide insights into the different structures of DNA. The vibrational modes of interest include the phosphate vibrational modes present in the lower wavenumber regions between 800 to 1250 cm^{-1}. Vibration modes between 800 and 1000 cm^{-1} shift in frequency with conformations of the sugar moieties, whereas modes between 1000 and 1250 cm^{-1} vary with the backbone main chain (C−O−P) conformation. Spectral features between 1250 and 1500 cm^{-1} are due to the sugar and nitrogenous-base ring vibrations, the base-sugar vibrations, and CH_3 bond vibrations at 1374 cm^{-1}.[48] Dehydration of DNA causes the major groove in the B-form to collapse, transforming it into the A-form, and these changes can be seen in the infrared spectrum.[48,51,52] Additionally, the spectral region between 1500 and 1800 cm^{-1} shows changes due to base-pairing and base-stacking and peak intensities can increase in this region, an indication of ssDNA.[48−51]

The solution-phase ATR-FTIR spectrum of the B-form shown in Figure 1b is in agreement with what has been previously observed for the different spectral features found for DNA.[28,49,50,53] A distinct peak at 1223 cm^{-1} due to the asymmetric phosphate stretching and the symmetric phosphate

https://doi.org/10.1021/acs.langmuir.4c02501
Langmuir 2024, 40, 27194−27205

stretching motion at 1085 cm^{-1} are both observed (Figure 1). Furanose vibrations occured at frequencies of 1019 and 1053 cm^{-1}, whereas DNA backbone and main chain vibrations were observed at 970 and 936 cm^{-1}. Additionally, C═O vibrations from nitrogenous bases (e.g., 1715 cm^{-1} for G) and ring C═N vibrations around 1608 cm^{-1} were also observed in the solution-phase B-form.[51] Upon drying, the A-form becomes apparent with the asymmetric phosphate stretching modes shifting to 1242 cm^{-1}, as well as changes observed in both peak frequencies and relative peak intensities, all which are in good agreement with previous studies.[48,51] In particular, sugar puckering modes of the C3′ endo confirmation in A-form were observed as a shoulder at 1178 cm^{-1}. Furanose vibrations and the symmetric phosphate stretching at 1085 cm^{-1} in the A-form appeared as a broad band with overlapping peaks instead of distinct sharp peaks as observed in the B-form. Moreover, a slight shift of backbone and main chain vibrations from 970 and 936 cm^{-1} in the B-form to 960 and 919 cm^{-1} in the A-form were observed due to the structural changes for the dehydrated form of DNA. Upon rehydration, the A-form regenerates back to the B-form as shown in SI−Figure S2.

The general spectral features of solution-phase ssDNA between 900 and 1300 cm^{-1} closely resemble many of the features observed for the B-form. However, there are some distinct differences in the spectra in the 1450−1800 cm^{-1} spectral range. For example, the intensities of the infrared peaks at 1603 and 1580 cm^{-1} corresponding to C═N vibrations of purines, particularly for G, were greatly enhanced for ssDNA due to the lack of hydrogen bonding interactions between G and C, and its impact on the vibrational mode intensities as has been previously discussed.[48,51] Therefore, peak intensity increases as well as distinct peaks at 1580 and 1603 cm^{-1} can be used as an indicator for the formation of ssDNA. Additionally, enhanced and overlapping bands in ssDNA were observed at 1657 and 1690 cm^{-1} and were assigned to the carbonyl C2═O2 vibration of T and C, respectively.[48,51]

An overall summary of the different vibrational frequencies and vibrational assignments for solution phase B-form, dried A-form, and solution phase ss-DNA is provided in Table 1. The table shows the vibrational frequencies associated with the different moieties within DNA. These assignments are based on the literature for solution phase DNA.

DNA Adsorption on α-FeOOH and α-Fe_2O_3 Surfaces. With this information from the solution phase spectra, the infrared spectra of DNA adsorbed on α-FeOOH and α-Fe_2O_3 surfaces from the aqueous phase at pH 5 are analyzed. These spectra are shown in Figure 2. In particular, Figure 2 shows spectra collected at the highest surface coverage following 1 h of DNA adsorption (*vide infra*) and compared to the spectrum for the B-form. The comparison shows that for DNA adsorbed on α-FeOOH, the adsorbed DNA spectrum closely resembles the solution-phase B-form spectrum, in agreement with earlier studies.[28] Despite this close agreement, there are some differences. These differences include an increase in intensity of the peak at 1653 cm^{-1} relative to the peak at 1715 cm^{-1} for DNA adsorbed on α-FeOOH. Both of these peaks correspond to C═O vibrations in G-C base pair.[28,49,50,53] Changes in the relative peak intensities have been observed previously for FTIR spectra of the B-form family, where the same structural form of DNA (e.g., B-form) produces minor variations in IR spectra in the base sensitive (~1500 to 1800 cm^{-1}) region. These changes have been attributed to small changes in the nitrogenous-base environment, and here these changes in the nitrogenous-base environment would be due to the interactions of DNA with the surface.[51]

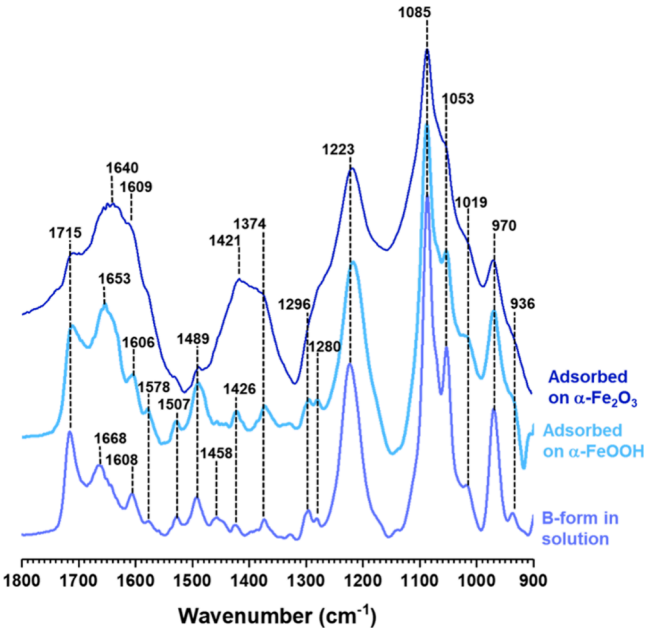

Figure 2. Comparison of normalized ATR-FTIR spectra of the B-form in solution with its adsorbed forms on α-FeOOH and α-Fe_2O_3 in the spectral region from 900 to 1800 cm^{-1} at an equilibrium surface coverage.

For DNA adsorbed on α-Fe_2O_3, the spectrum shows notable differences compared with the solution-phase B-form. In particular, there is a broadening of the peaks as well as changes in peak frequencies and intensities, especially in the spectral region extending from 1350 to 1475 cm^{-1} (Figure 2). The overall intensity increase in this region may indicate possible interactions of nitrogenous bases with α-Fe_2O_3 surface.[48] Previous studies have shown significant increases in the intensity of peaks at 1362 and 1412 cm^{-1} for adsorbed dGMP on oxide surfaces (e.g., TiO_2), suggesting the reason for the increase in intensity of these peaks on α-Fe_2O_3 is due to G base surface interactions.[30] In addition, nucleotide adsorption has been suggested to occur through the phosphate group on α-Fe_2O_3 via monodentate coordination whereas on α-FeOOH surfaces, bidentate coordination was preferred.[29] These binding mode preferences can potentially affect the rigidity of the adsorbed DNA on the surface. Assuming the initial DNA binding onto α-Fe_2O_3 surfaces undergoes via monodentate coordination, the mobility of adsorbed DNA on α-Fe_2O_3 surfaces may be higher than that of on α-FeOOH (Scheme 1). Higher mobility and spatial arrangements allow adsorbed DNA to further interact with the α-Fe_2O_3. The nitrogenous bases of DNA, particularly G and A (purines) can interact with surface sites on α-Fe_2O_3 via the $-NH_2$ group. Amine groups are known to interact with iron oxide surfaces through Lewis acid−base interactions.[55] Indeed, it has been shown that purines have a higher affinity on α-Fe_2O_3 surfaces.[30] Additionally, interactions with the $-NH_2$ groups from the base pairs in DNA and surface atoms have been computationally shown to be energetically feasible.[34] While these simulations were conducted for a very different mineral, calcite, the simulations showed that base interactions with surfaces were primarily driven by $-NH_2$ group and involve G,

https://doi.org/10.1021/acs.langmuir.4c02501
Langmuir 2024, 40, 27194−27205

Scheme 1. Conceptual Diagram Illustrating the Possible Interactions between DNA and α-Fe_2O_3 Surfaces[a]

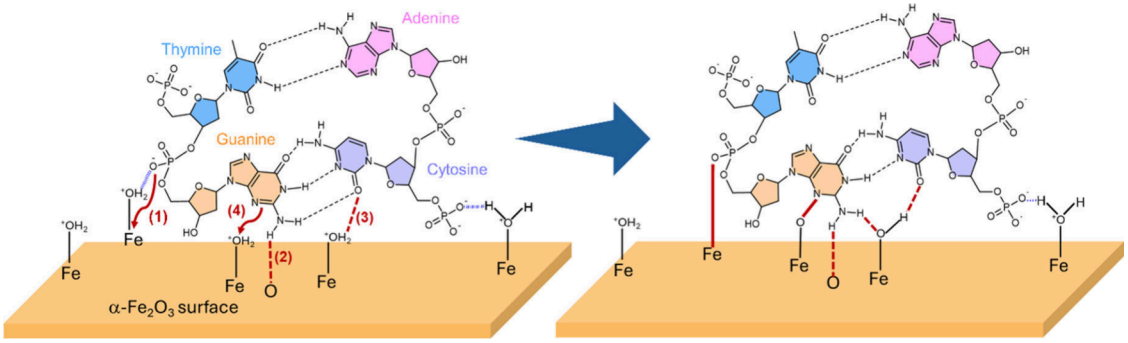

[a]Due to interactions of $-NH_2$ of bases with α-Fe_2O_3 surfaces, some of the H-bonds keeping the double-helix intact are disrupted. The possible interactions are (1) DNA undergoes monodentate binding via phosphate group on α-Fe_2O_3 surfaces and (2) the available H of $-NH_2$ group from G and possibly from A forms more H-bonds with surface O atoms. (3) More H-bonds between carbonyl O of C and surface hydroxyl groups are also possible. (4) Finally, the C═N from the purine ring of G can interact with positively charged surface hydroxyl groups (adsorbed water), thereby forming a N−O−Fe bonding interaction.

C, and A bases but not T. Freeman et al. have shown that these interactions induce both weak and massive helical structure disruptions primarily due to a general loss of interhelical H-bonds.[34] Similar interactions of DNA on α-Fe_2O_3 surfaces are plausible, thus giving rise to the changes in the infrared spectra that are suggested to be a slightly distorted B-form on the surface, as observed in ATR-FTIR spectra. Interestingly, DNA adsorbed on α-FeOOH surfaces does not indicate such base interactions with the surface.

To further examine the nature of these interactions, ATR-FTIR spectra of DNA dehydration on these surfaces were compared. Upon drying, adsorbed DNA on both surfaces produced spectral features resembling and consistent with the dehydrated A-form of DNA (Figure 3). The dried DNA spectrum on α-FeOOH appears to be the same as that of the dried A-form from solution. This suggests no difference in the changes of the helical structure for a dried DNA thin film

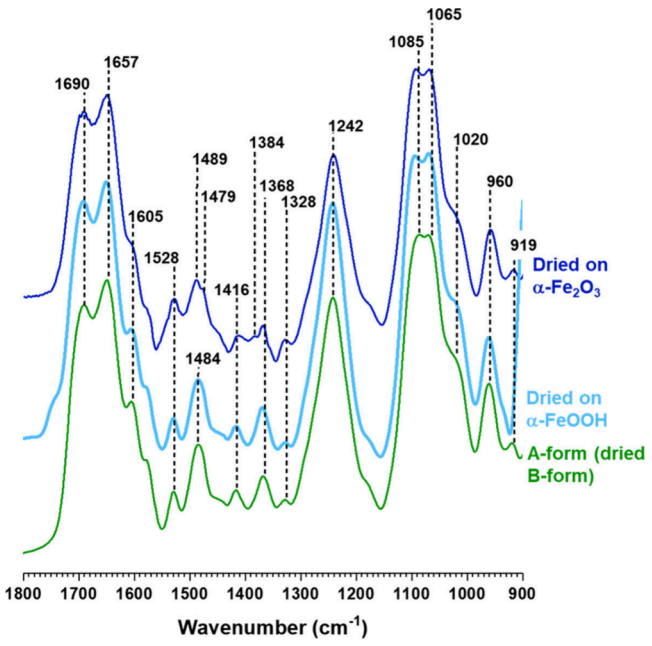

Figure 3. ATR-FTIR spectra in the spectral region from 900 to 1800 cm^{-1} of a DNA thin film dried onto ATR crystal (A-form), compared to adsorbed DNA dried on α-FeOOH and α-Fe_2O_3.

compared to DNA adsorbed on α-FeOOH. However, the spectrum for dried DNA when adsorbed on α-Fe_2O_3 shows some differences in peak frequencies and intensities in the spectral region from 1350 to 1550 cm^{-1} corresponding to nitrogenous-base vibrations. These changes include the appearance of two peaks at 1479 and 1489 cm^{-1} instead of a single peak at 1484 cm^{-1} in the A-form and the appearance of new peaks at 1384 and 1356 cm^{-1}. These changes can be attributed to changes in the nitrogenous-base ring vibrations which suggests again possible interactions of DNA bases with α-Fe_2O_3 surface.[48] Apart from these interactions, the spectra suggest that the double-helical structure remains intact on α-Fe_2O_3. Furthermore, the adsorbed DNA A-form rehydrates to the B-form when the aqueous solution is reintroduced into the ATR-FTIR cell at pH 5 (SI−Figure S2). On both α-FeOOH and α-Fe_2O_3 surfaces, adsorbed DNA did not significantly desorb following adsorption upon flowing pH 5 aqueous solution with no DNA (Figure 4, SI−Figure S3), indicating that DNA was irreversibly adsorbed at pH 5.

As shown in Scheme 1 several types of interactions are possible between DNA and α-Fe_2O_3 surfaces to further understand changes from the B- and A-forms. (1) DNA undergoes monodentate binding via phosphate group on α-Fe_2O_3 surfaces, and (2) the available H of the $-NH_2$ group from G and possibly from A forms more H-bonds with surface O atoms. (3) More H-bonds between carbonyl O of C and surface hydroxyl groups are also possible. (4) Finally, the C═N from purine ring of G can interact with positively charged surface hydroxyl groups (adsorbed water), thereby forming a N−O−Fe bond. Here, the complexity of the nature of interactions between the surface and DNA may disrupt some of the existing H-bonds in the double helix and induce formation of new H-bonds between $-NH_2$ and C═O groups from DNA with the surface. Changes in spectral features in the purine ring vibrations for DNA adsorbed on α-Fe_2O_3 (Figure 2) indicate additional interactions with the surface and N−O−Fe bond formation. While DNA adsorbs primarily on α-FeOOH and α-Fe_2O_3 in the B-form, there are differences in how they interact with these surfaces, as determined by the difference in the vibrational spectra and, as discussed below, the impact of changes in solution phase pH and the thermal stability of the double helix structure with respect to strand

https://doi.org/10.1021/acs.langmuir.4c02501
Langmuir 2024, 40, 27194−27205

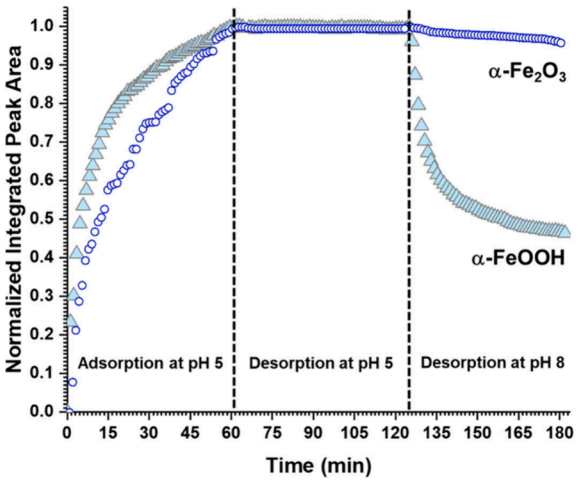

Figure 4. Normalized integrated peak area for the 1217 and 1222 cm^{-1} phosphate asymmetric stretching modes on α-FeOOH and α-Fe_2O_3, respectively, as a function of time showing lack of desorption of adsorbed DNA from α-FeOOH and α-Fe_2O_3 surfaces upon exposure to pH 5 saline solution and clear desorption (~55%) from α-FeOOH surfaces once exposed to pH 8 saline solution. DNA adsorbed on α-Fe_2O_3 shows minimal desorption (<5%) at pH 8.

separation for adsorbed DNA between these two surfaces and compared to DNA in solution.

Effect of pH on the Stability of Adsorbed DNA. In aqueous environments, since DNA has a high negative charge density of 2 elementary charges per 3.4 Å along the DNA axis due to its phosphates, they strongly interact with itself as well as with surrounding positively charged species while different segments of DNA repel from each other.[56] As the surface becomes more deprotonated, electrostatic interactions between DNA phosphate groups and the surface become weaker at higher pH conditions, thus causing adsorbed DNA to desorb. However, DNA may also exhibit much slower desorption kinetics compared to mononucleotides with increasing pH due to the multiple number of surface sites per DNA molecule. Following DNA adsorption at pH 5, the adsorbed DNA was then exposed to pH 8 and, subsequently, to pH 10 to investigate the stability of adsorbed DNA at the two higher pH values.

Figure 4 shows the normalized kinetics for DNA adsorption on α-FeOOH and α-Fe_2O_3 at pH 5 for 60 min. The time course ATR-FTIR spectra is shown in the SI—Figure S3. These data can be fit to a kinetic model. For both α-FeOOH and α-Fe_2O_3 surfaces, the initial DNA adsorption kinetics followed a pseudo-second-order (PSO) kinetics indicating strongly adsorbed DNA (see SI—Figure S4 and Eqs. S1 and S2 in SI).[57] Following 60 min of adsorption, a flow of saline solution at pH 5 without DNA was then introduced and the integrated peak area of the phosphate bands was plotted to determine if DNA desorbed from these particle surfaces following 65 min of flowing the saline solution over thin film of particles with adsorbed DNA. It can be seen that there is no desorption from the surface. Following this, at 125 min, the pH of the saline solution was increased to 8 and the flow continued for 55 min. It can be seen that changes in pH had no effect on DNA adsorption on α-Fe_2O_3 whereas for α-FeOOH, nearly 50% of the DNA desorbed from the surface as indicated by a decrease in the integrated peak area of the asymmetric phosphate stretching mode. Experiments involving DNA adsorption/desorption at pH 5 plus a solution pH 8 change were also conducted for an initial surface coverage of 50% on α-FeOOH. This was done following adsorption under the same conditions as shown in Figure 4 until time t = 7 min. At this time point half the surface coverage was obtained. A saline solution, i.e., 30 mM NaCl, at pH 5 was then introduced for 65 min followed by a saline solution of pH 8. Under these conditions, there was little desorption of DNA at this lower concentration

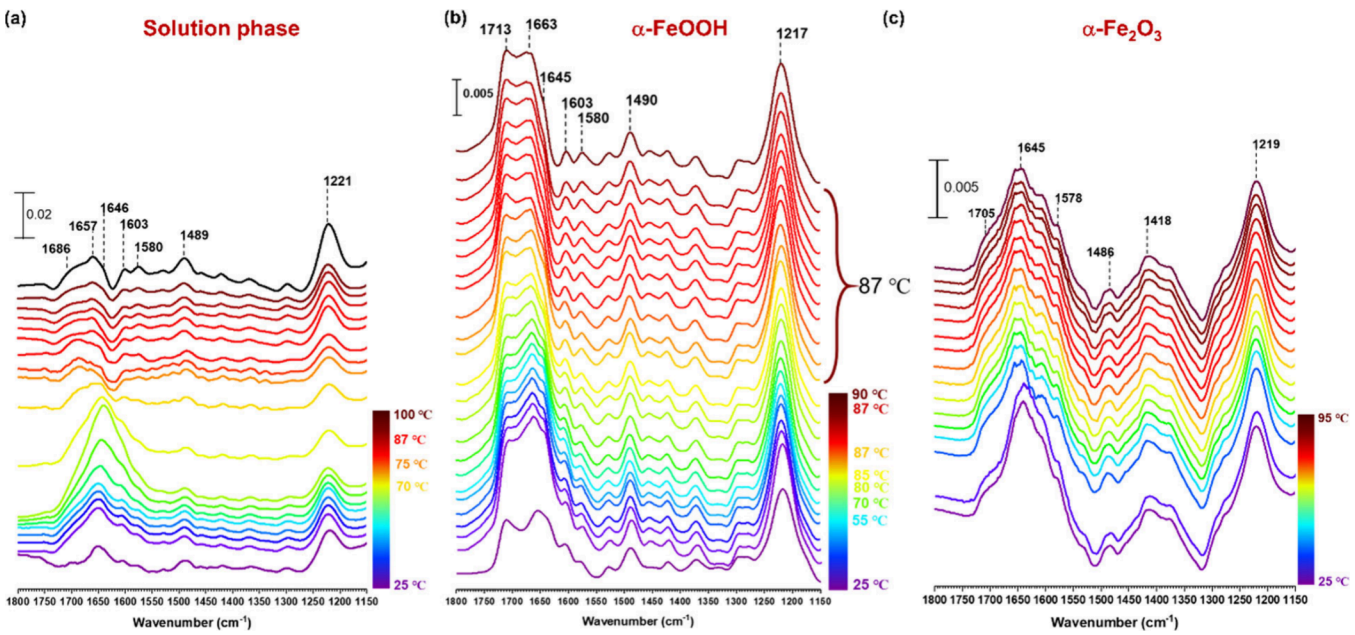

Figure 5. ATR-FTIR spectra for melting kinetics of DNA in the spectral range extending from 1150 to 1800 cm^{-1} (a) in solution, adsorbed on (b) α-FeOOH and (c) α-Fe_2O_3 at temperatures from 25 to 100 °C. Spectra were recorded continuously and reported at 5 °C increments starting at 25 °C, with the exception of including 87 °C. For solution phase, the topmost black spectrum was collected by DNA thermal denaturation in a flask and used as the standard for comparing with DNA spectra collected on the HATR apparatus.

https://doi.org/10.1021/acs.langmuir.4c02501
Langmuir 2024, 40, 27194−27205

(SI−Figure S5a). Therefore, roughly half of the adsorbed DNA at equilibrium on α-FeOOH (Figure 4) surfaces is impacted by pH and easily desorbs upon exposure to pH 8. However, multilayer adsorption is unlikely due to the irreversible adsorption observed at pH 5. In contrast to α-FeOOH surfaces, on α-Fe_2O_3 surfaces, adsorbed DNA showed minimal desorption (<5%) upon exposure to pH 8 or even going as high as pH 10. As pzc values for α-FeOOH and α-Fe_2O_3 are ∼8.4 and ∼7.0, respectively, at pH 8, α-FeOOH surfaces are transitioning from protonated to a deprotonated surface, whereas α-Fe_2O_3 surfaces are fully deprotonated. The impact of increasing the pH from 5 to 8 on adsorbed DNA differs between the two surfaces. If only the pzc was considered, it would be expected that DNA adsorbed on α-Fe_2O_3 would be most impacted as the charge would be negative. Therefore, the interactions between DNA and these surfaces are more complex than those from electrostatics alone.

Effect of Temperature on Stability of Adsorbed DNA. The melting temperature, T_m, is defined as the temperature at which half of the DNA molecules form ssDNA state.[41] The melting temperature width (ΔT) is the temperature range in which melting occurs. T_m depends on several factors including the length of DNA strand as shorter fragments will melt at lower temperatures,[58−60] the number of GC base pairs (i.e., number of H-bonds),[41,59] the salt concentration,[41] and overall nucleotide composition and sequence.[60−62] For most DNA, T_m lies between 50 and 100 °C, and for herring testes DNA, it is reported to be on average of 70 °C.[63,64] These variations for T_m can be attributed to differences in the experimental conditions and the length of the DNA extracted.

Figure 5a shows the ATR-FTIR spectra of solution-phase DNA at temperatures between 25 and 100 °C. The topmost black spectrum shows the ssDNA spectrum of thermally denatured DNA. Around 70 °C, the spectral features corresponding to thermally denatured DNA, such as more resolved peaks at 1580 and 1603 cm^{-1}, can be observed (Figure 5a and SI−Figure S6a). In comparison to the solution phase, DNA adsorbed on α-FeOOH (Figure 5b and SI−Figure S7) melting signatures starts to appear around 85 °C, and a steep resolution of the peaks at 1580 and 1603 cm^{-1} was seen during the equilibrium at 87 °C. Additionally, the peak at 1713 cm^{-1} corresponding to C═O of GC pairs remained resolved, whereas for the solution phase, a gradual disappearance of this peak was observed. Moreover, the adsorption of ssDNA shows a strong peak at 1713 cm^{-1} (SI−Figure S6b). In contrast to α-FeOOH, adsorbed DNA on α-Fe_2O_3 showed minimal melting signatures upon heating (Figure 5c and SI−Figure S6c). Instead of producing more resolved spectral features at 1580 and 1603 cm^{-1}, these features were slightly enhanced. Moreover, peak broadening in the spectral region from 1525 to 1725 cm^{-1} was seen, particularly ∼1705 cm^{-1} as early as 50 °C. Additionally, adsorption of ssDNA on α-Fe_2O_3 shows a strong peak at 1705 cm^{-1} and enhanced peaks at 1603 and 1580 cm^{-1}, in accordance with spectra of melted DNA adsorbed on α-Fe_2O_3. Once more, these differences observed in infrared spectra indicate the mineralogy-driven differences in interactions between DNA and the iron oxide surface.

The DNA melting curves generated from the ATR-FTIR spectra for solution phase and adsorbed on α-FeOOH and α-Fe_2O_3 surfaces are provided in Figure 6. Two assumptions were made when determining T_m. These are (i) all DNA are in the dsDNA state at 25 °C and (ii) only two states exist, where DNA is present as dsDNA or ssDNA.[43] Normalized ATR-FTIR spectral data extending from 900 to 1800 cm^{-1} were used in the SVD and principle component analysis. The determined T_m values for solution phase and DNA adsorbed on α-FeOOH and α-Fe_2O_3 are 70, 76, and 60 °C, respectively. Our solution phase data were best fit to Boltzmann two-state model (R^2 = 0.958), indicating DNA stays in dsDNA ⇌ 2ssDNA equilibrium, and T_m is in good agreement with previous T_m determinations of herring testes DNA.[63,64] The ΔT for solution phase was between ∼55 and 80 °C, 25 °C, and is also in good agreement with the previous studies.[63−65] Observed ΔT in these studies are ∼60−82 °C; 22 °C,[63] ∼55−85 °C; 30 °C,[65] and ∼50−80 °C; 30 °C.[64]

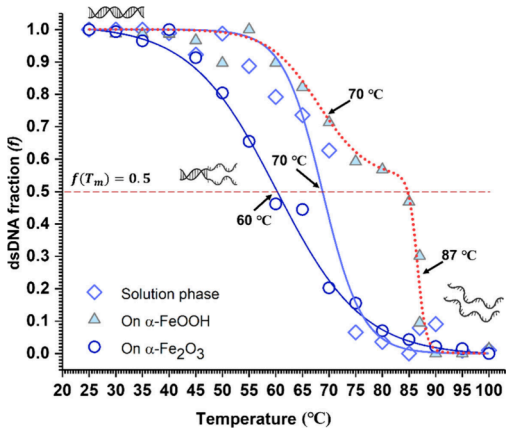

Figure 6. Normalized DNA melting curves generated by SVD analysis of normalized temperature dependent ATR-FTIR spectra for DNA in solution, adsorbed on α-FeOOH and on α-Fe_2O_3. The singular values from SVD analysis provide information about overall variations in the matrix/spectral data, whereas the right singular vectors provide temperature dependent variations corresponding to each singular value. The raw data were fit to the two-state Boltzmann model (solid lines), and T_m at which dsDNA fraction = ssDNA fraction = 0.5 was recorded. For α-FeOOH, the dotted line represents a biphase dose−response fit, suggesting that the DNA adsorbed on α-FeOOH deviates from the two-state Boltzmann model and follows a two-phase/multistate melting behavior. Formulas used and details of the Boltzmann and biphase dose−response fit functions are provided in the Supporting Information.

Although the adsorbed DNA melting temperature started at ∼60 °C on α-FeOOH, a rapid transition at 87 °C completed the melting. For all other holds of temperatures, such DNA melting nature at a particular temperature during the 600 s equilibrium was not observed. Moreover, DNA melting on α-FeOOH was best fit to the biphase dose−response fit (dash line in Figure 6) instead of the two-state Boltzmann fit, indicating more complex two-phase/multistate melting behavior. A presence of an intermediate state with both dsDNA and ssDNA portions present in the same DNA molecule and distinct DNA- α-FeOOH binding interactions as seen with desorption studies at pH 8 (Figure 4) as well can contribute to this two-phasic melting behavior. Although the T_m for DNA adsorbed on α-FeOOH can be reported as 76 °C with a more conventional approach, that is, according to two-state Boltzmann fit, a multistate/two-phasic melting behavior observed here can be analyzed as two distinct stages. From our data, the T_m^I for the first phase is 70 °C which is consistent with the solution phase, thus suggesting a more solution-like melting behavior. The second phase of the melting has T_m^{II} of 87 °C, and a much sharper ΔT, reflecting the DNA-α-FeOOH interactions similar to immobilized DNA on nanoparticle

https://doi.org/10.1021/acs.langmuir.4c02501
Langmuir 2024, 40, 27194−27205

Scheme 2. Conceptualized Diagram of Showing Different Melting Behaviors of Adsorbed DNA[a]

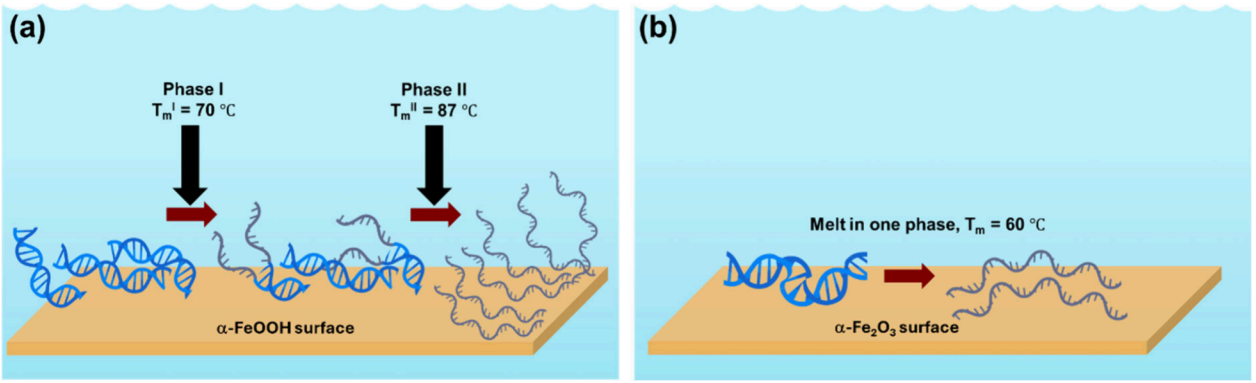

[a](a) On α-FeOOH there is a two-phase/multistate melting behavior with two distinct melting characteristics: (i) adsorbed DNA that melts at a similar temperature to solution phase DNA and (ii) adsorbed DNA that melts at higher temperatures. (b) On α-Fe_2O_3 surfaces leading to a singular melting behavior but at lower temperatures compared to solution phase.

systems.[66] Therefore, the melting behavior of adsorbed DNA on α-FeOOH suggests that DNA interacts with the surface in such a manner, giving it two distinct characters: one that is weakly adsorbed and the other more strongly adsorbed. Moreover, the melting curve of the adsorbed DNA on α-FeOOH with partial coverage of 50% showed a prominent second melting phase at 85 °C (strongly bound DNA) with a modest first melting phase at 69 °C (weakly adsorbed DNA) (SI−Figure S5b). Thus, the adsorbed DNA on α-FeOOH exhibits at least two distinct interactions (Scheme 2).

The melting temperature of DNA largely depends on the length of the DNA and the base-stacking and hydrogen-bonding interactions between strands, whereas ΔT is indicative of DNA length as well as the interactions DNA has with its sorrounding.[41,59] The ΔT of adsorbed DNA on α-Fe_2O_3 surfaces was observed between ∼45 and 90 °C, which is broader than the solution phase. DNA adsorbed on α-Fe_2O_3 surfaces also melts at a lower temperature, suggesting a destabilized and disrupted helical structure due to reduced number of H-bonds between the two strands and the additional interactions with the surface. This observation further confirms that during adsorption, DNA interacts with the α-Fe_2O_3 surface in such a way that the H-bonds that are keeping the double helix together are partially disrupted (Scheme 1). Overall, our study reports that DNA interactions with environmentally relevant interfaces are impacted by the nature of the mineral itself and the environment that they are present. Therefore, it underscores the importance of the scrutinizing the DNA-environmental studies with a more focus on mineralogy-driven DNA reactivity and retention pathways to further our knowledge and to develop method-diverse eDNA detection and monitoring tools.

CONCLUSION

DNA adsorption on mineral surfaces present in the environment can alter its structure and stability, as well as its reactivity. Here, herring testes DNA (∼1000 base pairs) was used as a model system to understand DNA adsorption and stability on two commonly present iron oxides in natural environments, α-FeOOH and α-Fe_2O_3. The ATR-FTIR spectra suggest that DNA adsorbs on both α-FeOOH and α-Fe_2O_3 surfaces in the B-form. DNA adsorbed on α-FeOOH surfaces, owing to possible bidentate coordination through the phosphate groups, shows the B-form structure remains intact. However, on α-Fe_2O_3 there is some distortion, possibly due to monodentate coordination through the phosphate groups and with nitrogen-bases interacting with the surface as well. Adsorbed DNA did not desorb upon exposure to pH 5 aqueous solutions, indicating strongly adsorbed DNA on both surfaces. The stability of adsorbed DNA on both iron oxide phases to higher pH and temperature was determined. Once exposed to higher pH (pH 8), adsorbed DNA readily desorbs from α-FeOOH (∼55%), further confirming the importance of protonation state, surface charge (electrostatics), and the nature of adsorption interactions. Although increased T_m of adsorbed DNA on α-FeOOH (76 °C) compared with that of solution phase (70 °C), according to more conventional two-state Boltzmann fit, was determined, the melting of adsorbed DNA shows two-phase/multistate behavior with two distinct characters, (i) weakly adsorbed (T_m^I = 70 °C) and (ii) strongly adsorbed and immobilized (T_m^{II} = 87 °C), with the latter showing a much sharper melting width (ΔT). This is indicative that the DNA adsorption on α-FeOOH follows at least two distinct interactions with the surface, and surface coverage is higher on α-FeOOH when normalized to surface area, compared to α-Fe_2O_3 surfaces. In contrast to α-FeOOH surfaces, on α-Fe_2O_3 surfaces, possibly due to the preference for monodentate binding via phosphate groups to the oxide surface, a greater mobility for adsorbed DNA is available to undergo further interactions with the surface. α-Fe_2O_3 surface interactions with DNA through the $-NH_2$ group is evident as observed by the ATR-FTIR peak enhancements at 1421 and 1374 cm^{-1} upon adsorption. A minimal desorption (<5%) at higher pH (8 and 10) was also observed, suggesting interactions present beyond electrostatic. Moreover, a decrease in T_m (60 °C) compared to that of solution phase was observed, indicating the loss of interstrand H-bonds during the surface adsorption. This is because the interactions between $-NH_2$ groups in the base pairs of DNA molecules with α-Fe_2O_3 surface lead to the formation of Fe−O−N bonds and H-bonds between the DNA and α-Fe_2O_3 surface at the cost of disrupting H-bonds that held the DNA double helix together. However, as all interstrand H-bonds are not disrupted, the double helix structure remains in a distorted B-form in adsorbed state.

Overall, our findings further confirm that eDNA interactions are highly mineral-specific. Mineral-bound eDNA in particular poses challenges in their detection and monitoring, causing

https://doi.org/10.1021/acs.langmuir.4c02501
Langmuir 2024, 40, 27194−27205

reduced accuracy and sensitivity, yet mineral-rich environments like sediments, soils, and aquatic habitats are effective at accumulating eDNA. Current challenges in detection and monitoring of mineral-bound eDNA include varying degradation rates upon adsorption, limitations in amplification due to the unavailability of binding sites on DNA molecules, reduced recovery, and coextraction of other substances/contaminants. Understanding eDNA adsorption/desorption on specific minerals allows us to optimize sampling parameters such as season, time of day, pH, and temperature and to maximize eDNA yield and improve data interpretation. Knowledge of eDNA desorption and stability on different minerals helps us to identify mineral systems contributing to legacy DNA: the DNA of a past species adsorbed and retained on minerals, increasing the accuracy of interpretation of the monitored data. Additionally, such knowledge on DNA adsorption/desorption on minerals can be extended to develop sequential extraction methods to minimize the coextraction of inhibitors species during eDNA amplification step of eDNA-based species detection: e.g., determining the eDNA desorption pHs for different minerals. Moreover, information on mineral-bound eDNA degradation can be utilized to further analyze the degraded products, which by extension can be used to design primers targeting these DNA fragments during the detection. Such approaches improve the sensitivity of existing eDNA-based detection tools.

In summary, developing method-diverse eDNA detection and monitoring tools for mineral-bound eDNA requires tailored eDNA extraction protocols for specific mineral systems to improve recovery and minimize DNA damage and contamination. The current study set out to answer several questions as it relates to changes to the DNA structure when adsorbed, the impact of changes in solution pH on adsorbed DNA stability, changes in thermal stability of adsorbed DNA compared to solution phase, and whether these changes were controlled by mineral specific interactions. Overall, this study underscores the importance of further addressing mineral-specific DNA interactions to better understand eDNA and how surfaces impact its stability. As shown here, there are very distinct differences between DNA and these two iron oxide phases.

■ ASSOCIATED CONTENT

Supporting Information

The Supporting Information is available free of charge at https://pubs.acs.org/doi/10.1021/acs.langmuir.4c02501.

Results of maximum surface coverage analysis; ATR-FTIR spectra of DNA solution phase, adsorbed on α-FeOOH and α-Fe_2O_3 surfaces for initial, once dried, and when rehydrated; spectra and analysis of adsorption kinetics; spectra and analysis related to DNA adsorption at half coverage on α-FeOOH; a comparison of dsDNA, melted adsorbed DNA, and adsorbed ssDNA; formulas for Boltzmann fit and biphase dose−response fit (PDF)

■ AUTHOR INFORMATION

Corresponding Author

Vicki H. Grassian − *Department of Chemistry and Biochemistry, University of California San Diego, La Jolla, California 92093, United States;* orcid.org/0000-0001-5052-0045; Email: vhgrassian@ucsd.edu

Author

Eshani Hettiarachchi − *Department of Chemistry and Biochemistry, University of California San Diego, La Jolla, California 92093, United States;* orcid.org/0000-0003-4293-770X

Complete contact information is available at: https://pubs.acs.org/10.1021/acs.langmuir.4c02501

Notes

The authors declare no competing financial interest.

■ ACKNOWLEDGMENTS

The research reported here was funded in whole or in part by the Army Research Office/Army Research Laboratory via Grant W911NF-23-1-0181 to the University of California, San Diego. Any errors and opinions are not those of the Army Research Office or Department of Defense and are attributable solely to the authors. E.H. thanks and acknowledges Cholaphan Deeleepojananan, David Hunter, Debolina Sarkar, An Hsieh, Hoang Phuong My Nguyen, and Qishan (Lisa) Liang for helpful discussions. V.H.G. thanks Professor Alexis Komor for helpful discussions. TOC graphics, Figures 1 and 6, SI−Figure S5 and Scheme 2 contain elements that are created with BioRender.com.

■ REFERENCES

(1) Jo, T.; Takao, K.; Minamoto, T. Linking the State of Environmental DNA to Its Application for Biomonitoring and Stock Assessment: Targeting Mitochondrial/Nuclear Genes, and Different DNA Fragment Lengths and Particle Sizes. *Environ. DNA* **2022**, *4* (2), 271−283.

(2) Barnes, M. A.; Turner, C. R.; Jerde, C. L.; Renshaw, M. A.; Chadderton, W. L.; Lodge, D. M. Environmental Conditions Influence EDNA Persistence in Aquatic Systems. *Environ. Sci. Technol.* **2014**, *48* (3), 1819−1827.

(3) Rourke, M. L.; Fowler, A. M.; Hughes, J. M.; Broadhurst, M. K.; DiBattista, J. D.; Fielder, S.; Wilkes Walburn, J.; Furlan, E. M. Environmental DNA (EDNA) as a Tool for Assessing Fish Biomass: A Review of Approaches and Future Considerations for Resource Surveys. *Environ. DNA* **2022**, *4* (1), 9−33.

(4) Lynggaard, C.; Bertelsen, M. F.; Jensen, C. V.; Johnson, M. S.; Frøslev, T. G.; Olsen, M. T.; Bohmann, K. Airborne Environmental DNA for Terrestrial Vertebrate Community Monitoring. *Curr. Biol.* **2022**, *32* (3), 701−707.

(5) Pawlowski, J.; Bruce, K.; Panksep, K.; Aguirre, F. I.; Amalfitano, S.; Apothéloz-Perret-Gentil, L.; Baussant, T.; Bouchez, A.; Carugati, L.; Cermakova, K.; et al. Environmental DNA Metabarcoding for Benthic Monitoring: A Review of Sediment Sampling and DNA Extraction Methods. *Sci. Total Environ.* **2022**, *818*, 151783.

(6) Jo, T.; Minamoto, T. Complex Interactions between Environmental DNA (EDNA) State and Water Chemistries on EDNA Persistence Suggested by Meta-analyses. *Mol. Ecol. Resour.* **2021**, *21* (5), 1490−1503.

(7) Pawlowski, J.; Bonin, A.; Boyer, F.; Cordier, T.; Taberlet, P. Environmental DNA for Biomonitoring. *Mol. Ecol.* **2021**, *30* (13), 2931−2936.

(8) Takahashi, M.; Saccò, M.; Kestel, J. H.; Nester, G.; Campbell, M. A.; van der Heyde, M.; Heydenrych, M. J.; Juszkiewicz, D. J.; Nevill, P.; Dawkins, K. L.; et al. Aquatic Environmental DNA: A Review of the Macro-Organismal Biomonitoring Revolution. *Sci. Total Environ.* **2023**, *873*, 162322.

(9) Rishan, S. T.; Kline, R. J.; Rahman, M. S. Applications of Environmental DNA (EDNA) to Detect Subterranean and Aquatic Invasive Species: A Critical Review on the Challenges and Limitations of EDNA Metabarcoding. *Environ. Adv.* **2023**, *12*, 100370.

(10) Harrison, J. B.; Sunday, J. M.; Rogers, S. M. Predicting the Fate of EDNA in the Environment and Implications for Studying Biodiversity. *Proc. R. Soc. B Biol. Sci.* **2019**, *286* (1915), 20191409.
(11) Bass, D.; Christison, K. W.; Stentiford, G. D.; Cook, L. S. J.; Hartikainen, H. Environmental DNA/RNA for Pathogen and Parasite Detection, Surveillance, and Ecology. *Trends Parasitol.* **2023**, *39* (4), 285−304.
(12) Thomsen, P. F.; Willerslev, E. Environmental DNA - An Emerging Tool in Conservation for Monitoring Past and Present Biodiversity. *Biol. Conserv.* **2015**, *183*, 4−18.
(13) Mauvisseau, Q.; Harper, L. R.; Sander, M.; Hanner, R. H.; Kleyer, H.; Deiner, K. The Multiple States of Environmental DNA and What Is Known about Their Persistence in Aquatic Environments. *Environ. Sci. Technol.* **2022**, *56* (9), 5322−5333.
(14) Jo, T.; Murakami, H.; Masuda, R.; Minamoto, T. Selective Collection of Long Fragments of Environmental DNA Using Larger Pore Size Filter. *Sci. Total Environ.* **2020**, *735*, 139462.
(15) Jo, T.; Arimoto, M.; Murakami, H.; Masuda, R.; Minamoto, T. Particle Size Distribution of Environmental DNA from the Nuclei of Marine Fish. *Environ. Sci. Technol.* **2019**, *53* (16), 9947−9956.
(16) Lamb, P. D.; Fonseca, V. G.; Maxwell, D. L.; Nnanatu, C. C. Systematic Review and Meta-analysis: Water Type and Temperature Affect Environmental DNA Decay. *Mol. Ecol. Resour.* **2022**, *22* (7), 2494−2505.
(17) Wilcox, T. M.; McKelvey, K. S.; Young, M. K.; Lowe, W. H.; Schwartz, M. K. Environmental DNA Particle Size Distribution from Brook Trout (Salvelinus Fontinalis). *Conserv. Genet. Resour.* **2015**, *7* (3), 639−641.
(18) Turner, C. R.; Barnes, M. A.; Xu, C. C. Y.; Jones, S. E.; Jerde, C. L.; Lodge, D. M. Particle Size Distribution and Optimal Capture of Aqueous Macrobial EDNA. *Methods Ecol. Evol.* **2014**, *5* (7), 676−684.
(19) Romanowski, G.; Lorenz, M. G.; Wackernagel, W. Adsorption of Plasmid DNA to Mineral Surfaces and Protection against DNase I. *Appl. Environ. Microbiol.* **1991**, *57* (4), 1057−1061.
(20) Hou, Y.; Wu, P.; Zhu, N. The Protective Effect of Clay Minerals against Damage to Adsorbed DNA Induced by Cadmium and Mercury. *Chemosphere* **2014**, *95*, 206−212.
(21) Scappini, F.; Casadei, F.; Zamboni, R.; Franchi, M.; Gallori, E.; Monti, S. Protective Effect of Clay Minerals on Adsorbed Nucleic Acid against UV Radiation: Possible Role in the Origin of Life. *Int. J. Astrobiol.* **2004**, *3* (1), 17−19.
(22) Bradford, S. A.; Morales, V. L.; Zhang, W.; Harvey, R. W.; Packman, A. I.; Mohanram, A.; Welty, C. Transport and Fate of Microbial Pathogens in Agricultural Settings. *Crit. Rev. Environ. Sci. Technol.* **2013**, *43* (8), 775−893.
(23) Cai, P.; Huang, Q.; Zhang, X.; Chen, H. Adsorption of DNA on Clay Minerals and Various Colloidal Particles from an Alfisol. *Soil Biol. Biochem.* **2006**, *38* (3), 471−476.
(24) Saladino, R.; Crestini, C.; Neri, V.; Brucato, J. R.; Colangeli, L.; Ciciriello, F.; Di Mauro, E.; Costanzo, G. Synthesis and Degradation of Nucleic Acid Components by Formamide and Cosmic Dust Analogues. *ChemBioChem* **2005**, *6* (8), 1368−1374.
(25) Saladino, R.; Neri, V.; Crestini, C.; Costanzo, G.; Graciotti, M.; Di Mauro, E. Synthesis and Degradation of Nucleic Acid Components by Formamide and Iron Sulfur Minerals. *J. Am. Chem. Soc.* **2008**, *130* (46), 15512−15518.
(26) Salter, I. Seasonal Variability in the Persistence of Dissolved Environmental DNA (EDNA) in a Marine System: The Role of Microbial Nutrient Limitation. *PLoS One* **2018**, *13* (2), No. e0192409.
(27) James Cleaves, H.; Crapster-Pregont, E.; Jonsson, C. M.; Jonsson, C. L.; Sverjensky, D. A.; Hazen, R. A. The Adsorption of Short Single-Stranded DNA Oligomers to Mineral Surfaces. *Chemosphere* **2011**, *83* (11), 1560−1567.
(28) Schmidt, M. P.; Martínez, C. E. Ironing Out Genes in the Environment: An Experimental Study of the DNA-Goethite Interface. *Langmuir* **2017**, *33* (34), 8525−8532.
(29) Sit, I.; Young, M. A.; Kubicki, J. D.; Grassian, V. H. Distinguishing Different Surface Interactions for Nucleotides Adsorbed onto Hematite and Goethite Particle Surfaces through ATR-FTIR Spectroscopy and DFT Calculations. *Phys. Chem. Chem. Phys.* **2023**, *25* (30), 20557−20566.
(30) Sit, I.; Quirk, E.; Hettiarachchi, E.; Grassian, V. H. Differential Surface Interactions and Surface Templating of Nucleotides (DGMP, DCMP, DAMP, and DTMP) on Oxide Particle Surfaces. *Langmuir* **2022**, *38* (49), 15038−15049.
(31) Vlasova, N. N.; Markitan, O. V. Adsorption of Pyrimidine Nucleotides on a Titanium Dioxide Surface. *Colloid J.* **2018**, *80* (4), 364−370.
(32) Vlasova, N. N.; Markitan, O. V. Adsorption Complexes of Purine Nucleotides on a Titanium Dioxide Surface. *Colloid J.* **2019**, *81* (1), 14−20.
(33) Vlasova, N.; Markitan, O. Phosphate-Nucleotide-Nucleic Acid: Adsorption onto Nanocrystalline Ceria Surface. *Colloids Surfaces A Physicochem. Eng. Asp.* **2022**, *648*, 129214.
(34) Freeman, C. L.; Dieudonné, L.; Agbaje, O. B. A.; Žure, M.; Sanz, J. Q.; Collins, M.; Sand, K. K. Survival of Environmental DNA in Sediments: Mineralogic Control on DNA Taphonomy. *Environ. DNA* **2023**, *5* (6), 1691−1705.
(35) Integrated Taxonomic Information System. https://www.itis.gov/ (accessed Sep 9, 2024).
(36) Fishbase. https://fishbase.de/ (accessed Sep 9, 2024).
(37) Kim, D.; Grassian, V. H. Attenuated Total Reflection-Fourier Transform Infrared and Atomic Force Microscopy-Infrared Spectroscopic Investigation of Suwannee River Fulvic Acid and Its Interactions with α-FeOOH. *ACS Earth Sp. Chem.* **2022**, *6* (1), 81−89.
(38) Jiao, Y.; Han, D.; Lu, Y.; Rong, Y.; Fang, L.; Liu, Y.; Han, R. Characterization of Pine-Sawdust Pyrolytic Char Activated by Phosphoric Acid through Microwave Irradiation and Adsorption Property toward CDNB in Batch Mode. *Desalin. WATER Treat.* **2017**, *77*, 247−255.
(39) Kosmulski, M. The PH-Dependent Surface Charging and Points of Zero Charge. *J. Colloid Interface Sci.* **2011**, *353* (1), 1−15.
(40) Liu, J. Adsorption of DNA onto Gold Nanoparticles and Graphene Oxide: Surface Science and Applications. *Phys. Chem. Chem. Phys.* **2012**, *14* (30), 10485.
(41) Khandelwal, G.; Bhyravabhotla, J. A Phenomenological Model for Predicting Melting Temperatures of DNA Sequences. *PLoS One* **2010**, *5* (8), No. e12433.
(42) Mudunkotuwa, I. A.; Minshid, A. Al; Grassian, V. H. ATR-FTIR Spectroscopy as a Tool to Probe Surface Adsorption on Nanoparticles at the Liquid-Solid Interface in Environmentally and Biologically Relevant Media. *Analyst* **2014**, *139* (5), 870−881.
(43) Menssen, R. J.; Tokmakoff, A. Length-Dependent Melting Kinetics of Short DNA Oligonucleotides Using Temperature-Jump IR Spectroscopy. *J. Phys. Chem. B* **2019**, *123* (4), 756−767.
(44) Hendler, R. W.; Shrager, R. I. Deconvolutions Based on Singular Value Decomposition and the Pseudoinverse: A Guide for Beginners. *J. Biochem. Biophys. Methods* **1994**, *28* (1), 1−33.
(45) Wall, M. E.; Rechtsteiner, A.; Rocha, L. M. Singular Value Decomposition and Principal Component Analysis. In *A Practical Approach to Microarray Data Analysis*; Kluwer Academic Publishers: Boston, MA; pp 91−109, DOI: 10.1007/0-306-47815-3_5.
(46) Sanstead, P. J.; Tokmakoff, A. Direct Observation of Activated Kinetics and Downhill Dynamics in DNA Dehybridization. *J. Phys. Chem. B* **2018**, *122* (12), 3088−3100.
(47) Project Jupyter. https://jupyter.org/.
(48) Banyay, M.; Sarkar, M.; Gräslund, A. A Library of IR Bands of Nucleic Acids in Solution. *Biophys. Chem.* **2003**, *104* (2), 477−488.
(49) Taillandier, E.; Liquier, J. Infrared Spectroscopy of DNA. *Methods Enzymol.* **1992**, *211*, 307−335.
(50) Parker, A. W.; Quinn, S. J. Infrared Spectroscopy of DNA. In *Encyclopedia of Biophysics*; Springer: Berlin, 2013; pp 1065−1074, DOI: 10.1007/978-3-642-16712-6_112.
(51) Mantsch, H. H.; Chapman, D. *Infrared Spectroscopy of Biomolecules*; Wiley-Liss Inc.: New York, 1996.

https://doi.org/10.1021/acs.langmuir.4c02501
Langmuir 2024, 40, 27194−27205

(52) Tinoco, I. Nucleic Acid Structures, Energetics, and Dynamics. *J. Phys. Chem.* **1996**, *100* (31), 13311−13322.
(53) Parikh, S. J.; Mukome, F. N. D.; Zhang, X. ATR-FTIR Spectroscopic Evidence for Biomolecular Phosphorus and Carboxyl Groups Facilitating Bacterial Adhesion to Iron Oxides. *Colloids Surfaces B Biointerfaces* **2014**, *119*, 38−46.
(54) Liquier, J.; Taillandier, E. Infrared Spectroscopy of Nucleic Acids. In *Infrared Spectroscopy of Biomolecules*; Mantsch, H. H., Chapman, D., Eds.; Wiley-Liss Inc.: New York, 1996; pp 131−158.
(55) Wielant, J.; Hauffman, T.; Blajiev, O.; Hausbrand, R.; Terryn, H. Influence of the Iron Oxide Acid-Base Properties on the Chemisorption of Model Epoxy Compounds Studied by XPS. *J. Phys. Chem. C* **2007**, *111* (35), 13177−13184.
(56) Rocha, M. S. Extracting Physical Chemistry from Mechanics: A New Approach to Investigate DNA Interactions with Drugs and Proteins in Single Molecule Experiments. *Integr. Biol.* **2015**, *7* (9), 967−986.
(57) Sahoo, T. R.; Prelot, B. Adsorption Processes for the Removal of Contaminants from Wastewater. In *Nanomaterials for the Detection and Removal of Wastewater Pollutants*; Elsevier, 2020; pp 161−222, DOI: 10.1016/B978-0-12-818489-9.00007-4.
(58) Pörschke, D. Cooperative Nonenzymic Base Recognition II. Thermodynamics of the Helix-coil Transition of Oligoadenylic + Oligouridylic Acids. *Biopolymers* **1971**, *10* (10), 1989−2013.
(59) Blake, R. D. Cooperative Lengths of DNA during Melting. *Biopolymers* **1987**, *26* (7), 1063−1074.
(60) Ussery, D. W. DNA Denaturation. In *Encyclopedia of Genetics*; Elsevier, 2001; pp 550−553, DOI: 10.1006/rwgn.2001.0353.
(61) Breslauer, K. J.; Frank, R.; Blöcker, H.; Marky, L. A. Predicting DNA Duplex Stability from the Base Sequence. *Proc. Natl. Acad. Sci. U. S. A.* **1986**, *83* (11), 3746−3750.
(62) Delcourt, S. G.; Blake, R. D. Stacking Energies in DNA. *J. Biol. Chem.* **1991**, *266* (23), 15160−15169.
(63) Ke, W.; Yu, D.; Wu, J. Raman Spectroscopic Study of the Influence on Herring Sperm DNA of Heat Treatment and Ultraviolet Radiation. *Spectrochim. Acta Part A Mol. Biomol. Spectrosc.* **1999**, *55* (5), 1081−1090.
(64) Shen, H.-Y.; Zhang, Y.; Lin, F.; Xu, N.-Y.; Zheng, H.-M. In Vitro Study on the Interactions between Native Herring Sperm DNA and Melamine in the Presence of Ca2+ by Spectroscopic and Voltammetric Techniques. *Int. J. Electrochem. Sci.* **2012**, *7* (5), 3817−3834.
(65) Zhong, W.; Yu, J.-S.; Liang, Y. Chlorobenzylidine-Herring Sperm DNA Interaction: Binding Mode and Thermodynamic Studies. *Spectrochim. Acta Part A Mol. Biomol. Spectrosc.* **2003**, *59* (6), 1281−1288.
(66) Sun, Y.; Harris, N. C.; Kiang, C. H. Melting Transition of Directly Linked Gold Nanoparticle DNA Assembly. *Phys. A Stat. Mech. its Appl.* **2005**, *350* (1), 89−94.

https://doi.org/10.1021/acs.langmuir.4c02501
Langmuir 2024, 40, 27194−27205